Available online at www.sciencedirect.com

SCIENCE DIRECT®

Tectonophysics 387 (2004) 169–187

TECTONOPHYSICS

www.elsevier.com/locate/tecto

Lower crust indentation or horizontal ductile flow during continental collision?

M. Gerbault[a,*], E. Willingshofer[b]

[a]LMTG IRD UR154, University Paul Sabatier, 14 av. Edouard Belin, 31400 Toulouse, France
[b]Vrije Univ. Amsterdam, De Boelelaan 1085, 1081 HV Amsterdam, Netherlands

Received 18 December 2002; accepted 2 June 2004

Abstract

Conditions for indentation and channelised flow are investigated with two-dimensional thermomechanical models of Alpine-type continental collision. The models mimic the development of an orogen at an initial central portion of weakened lithosphere 150 km wide, coherent with several geological reconstructions. We study in particular the role of lower crustal strength in developing peculiar geometries after 20 Ma of shortening at 1 cm/year. Crustal layers produce geometries of imbricate layers, which result from two contrasted mechanisms of either channelised ductile lateral flow or horizontal rigid-like indentation:

– Channelised lateral flow develops when the lateral lower crust has a viscosity less than 10^{21} Pa s, exhibiting velocities opposite to the direction of convergence. This mechanism of deformation produces subhorizontal shear zones at the boundaries between the lower crust and the more competent upper crust and lithospheric mantle. It is also associated with a topographic plateau that equilibrates with a wide (about 200 km) but quasi-constant crustal root about 50 km deep.
– In contrast, indentation occurs with lateral lower crust layers that have a viscosity greater than about 10^{23} Pa s, producing significant shortening and thickening of the central crust. In this case topography develops steep and narrow (around 100 km wide), associated with a thickened crust exceeding 60 km depth. A crustal-scale pop-up forms bounded by subvertical shear zones that root into the mantle lithosphere.

Keywords: Continental collision indentation; Channel flow; Lower crust; Elastic–viscous–plastic rheology

1. Introduction

While the capability of the lower continental crust to decouple mantle lithosphere and upper crust deformation is recognised as a key element to

* Corresponding author. Tel.: +33 5 61 33 26 39; fax: +33 5 61 33 25 60.
E-mail address: gerbault@lmtg.obs-mip.fr (M. Gerbault).

0040-1951/$ - see front matter © 2004 Elsevier B.V. All rights reserved.
doi:10.1016/j.tecto.2004.06.012

intracontinental orogeny, its mechanisms of deformation at the regional scale remain poorly constrained. In addition to constitutive laws derived from laboratory experiments on specific minerals, the behaviour of the lower crust can also be inferred from the interpretation of geological and geophysical data. Although exposures of lower crustal rocks are rare, observed imbrications of layers indicate a variety of contrasted rheologies that coexist and probably interact, simultaneously, during orogeny.

For example, the Central European Alps is a mountain belt for which good and reliable data are available, yet the deep structure of the chain remains a matter of controversy. Deep seismic reflection profiles reveal the presence of lower crustal wedges, which are considered as the expression of a strong lower crust; an interpretation that finds support by seismic activity down to Moho depths (e.g., Schmid and Kissling, 2000). However, both wedge-shaped structures and seismic activity at lower crustal levels do not unambiguously imply the presence of a strong lower crust. That is, the strong reflectivity of the lower crust may also be related to fluids (Klemperer, 1987 and references therein), which would also reduce the frictional strength and, hence, cause seismic activity where otherwise creep processes prevail (e.g., Deichmann, 1992). Furthermore, subduction of lower crust in collisional settings, as suggested for the Swiss Alps in Europe, is thought to be indicative of a strong lower crust, because it remains attached to the subducting mantle lithosphere (Pfiffner et al., 2000). In other collision zones, a weak lower crust rheology is suggested, as for the Tibetan plateau. Horizontal ductile channel flow in this lower crust could explain the discrepancy between convergence rate and the amount of surface deformation (e.g., Royden et al., 1997; Shen et al., 2001), as well as the particular seismic reflectivity of the lower crust (Ross et al., 2004).

The present study stands as preliminary and conceptual work to study the behaviour of the lower crust within Alpine-type collision tectonics. We perform lithospheric-scale 2D numerical models of continental collision using pressure and temperature dependent elastic, viscous and brittle rheologies (e.g., Ranalli, 1995), and a relatively large preexisting weak zone that forms the plate boundary (e.g., Thompson et al., 1997; Beaumont et al., 2000), in order to address key questions related to collision tectonics such as (1) What are the mechanical conditions for the occurrence of indentation (traditionally linked to a brittle and strong rheology) or horizontal channel flow (linked to low viscosity and weak rheology) in the lower crust? (2) Which typical strength and lengths are involved in lower crust horizontal flow and indentation, and (3) Can these mechanisms account for wedge geometries (‘crocodile’ structures) as inferred from reflection seismics or field observations?

2. Indentation vs. lateral flow—what does it mean?

Deformation resulting from rigid indentation is well described by the theory of plasticity in classical engineering mechanics (e.g., Hill, 1950), and was shown to apply to some extent to plate tectonics (e.g., Odé, 1960; Davy and Cobbold, 1988; Regenauer-Lieb, 1999). Considering the brittle behaviour of the upper crust, indentation of a continent by a rigid plate explains some of the large-strike slip features observed in major collision zones like in India–Asia (Tapponnier et al., 1982) or in the Eastern Alps (e.g., Ratschbacher et al., 1991a,b; Fig. 1a). Convergence between two plates induces *lateral extrusion* of rigid crustal blocks along curved slip-lines that eventually become perpendicular to the shortening direction.

However, the term lateral extrusion also refers to a nearly opposite mechanism of deformation, as it was defined by Bird (1991) as low-viscosity flow of the lower crust similar to a Poiseuille flow, in a direction opposite to the direction of convergence (Fig. 1b). One should recall Artyushkov’s (1973) note on the possibility for crustal material to spread horizontally in order to equilibrate buoyancy forces resulting from crustal thickness variations. A number of studies then used this argument to study extensional tectonics or mountain collapse for a viscous rheology (see review in McKenzie et al., 2000). Describing processes involved during orogeny, and using a vertically variable power-law rheology, Gratton (1989) used the term *buoyancy-driven creep*, as he derived scaling laws for orogenic growth, that

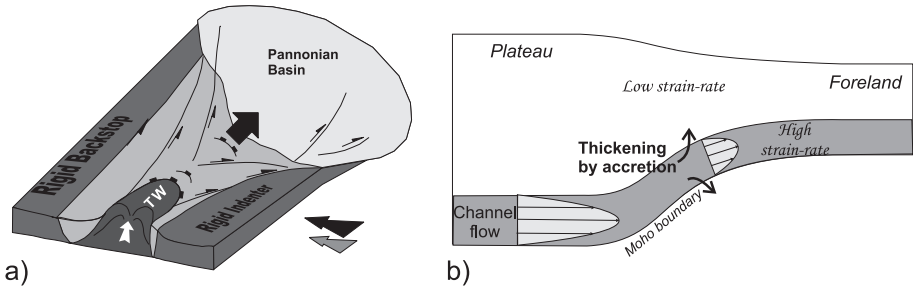

Fig. 1. One term for two different mechanisms of deformation: (a) lateral extrusion in plane view, material is squeezed from the sides by indenters, and along crustal-scale transform faults (modified from Ratschbacher et al., 1991b, showing extrusion of the Eastern Alps into the Pannonian basin). Tauern Window (TW). (b) Lateral extrusion in a vertical plane, of lower crust, forming a low viscosity channel in between the more competent upper mantle and upper crusts. This channel flow contributes to thickening from the edges of the orogen (modified from Clark and Royden, 2000; Medvedev and Beaumont, 2001).

relate the equations of equilibrium and isostasy, with the convergence rate.

As it was shown that lithospheric strength strongly depends on temperature, composition and strain rate (Goetze, 1978; Brace and Kohlstedt, 1980; Ord and Hobbs, 1989), many models have then explored the effects of mechanical decoupling between the crust and the mantle (e.g., Chery et al., 1991; Lobkovsky and Kerchmann, 1991; Burov and Diament, 1992; Avouac and Burov, 1996; Royden, 1996), and its relation to deformation at the surface. The mechanism of channelised flow in deep crustal levels was linked to the formation of high topographic plateaus. Royden et al. (1997) suggested that the little crustal shortening observed in Tibet since 4 Ma results from channelised flow in the lower crust, which decouples the upper crust from the 'faster moving' underlying mantle. More recently, the influence of surface denudation on exhumation of low-viscosity crustal channels was also investigated (Beaumont et al., 2001), and applied to the Himalayas.

In the following, we investigate conditions for which either indentation (intrusion of weak crust by stronger material coming from the external parts of an orogen), or channel flow (outward extrusion of weak crust) can occur in deep crustal levels. We display numerical models that account for the dynamical aspect of orogenic growth, including time-varying elastic, brittle and viscous rheologies. Since many previous studies have developed in detail analytical expressions of viscous deformation in the lower crust, we do not show any such equations here, all the more that the numerical models account for a self-consistent variation in time of topography and lithospheric layers.

3. Model setup

3.1. General features

We use a mixed finite-element/finite-differences thermomechanical code modified from Parovoz (Poliakov and Podladchikov, 1992). It is based on the Fast Lagrangian Analysis Continuum method (FLAC, Cundall and Board, 1988), which incorporates an explicit time-marching scheme, and allows the use of a wide range of constitutive laws such as brittle–elastic–ductile rheology derived by rock experimentalists (e.g., Brace and Kohlstedt, 1980; Ranalli, 1995). It handles initiation and propagation of non-predefined faults (shear bands). Parovoz has proved efficient in modelling many tectonic features, such as lithospheric rifting (Buck and Poliakov, 1998; Burov and Poliakov, 2001), lithospheric buckling (Gerbault et al., 1999) and continental subduction (Burov et al., 2001). Detailed features of the code can be found, e.g., in Gerbault et al. (2003).

The lithosphere is modelled as a medium of 300×30 quadrilateral elements, with a total length of 900 km and depth of 80 km (Fig. 2). Both lateral borders are free to slip vertically, and a horizontal velocity V_x=0.5 cm/year is applied on each side (compression rate=3×10^{-16}/s). The lithosphere floats on the asthenosphere within the gravity field; hydrostatic boundary conditions are applied at the bottom of

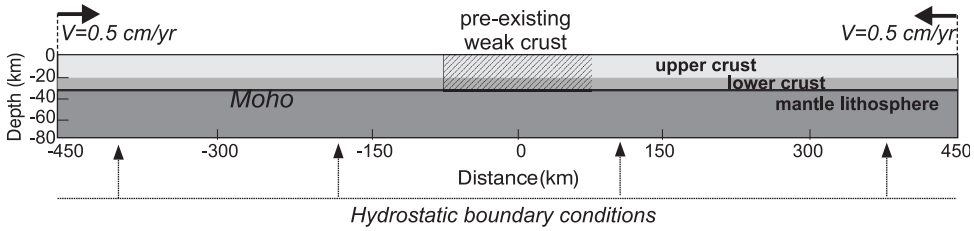

Fig. 2. General setup of models. Moho thickness is constant at 30 km depth. Buoyancy applies at 80 km depth. Free-slip conditions are applied on both sides of the model, and compression occurs at a constant total rate of 1 cm/year. In models M1, M2, M3, M5, the lower crust and upper crust have the same rheology. The 'preexisting weak crust' at the centre, 150 km long, has a specific colour to serve as a marker. In models M1 and M2, it has the same rheological properties as the rest of the crust, and has a specific rheology in models M3 and M4.

the model, with an underlying density of 3250 kg/m^3. The surface is stress free.

Surface processes are modelled with a diffusion equation (e.g., Avouac and Burov, 1996), so that the surface height h is modified according to $\mathrm{d}h/\mathrm{d}t=k_{\mathrm{er}}\mathrm{d}h^2/\mathrm{d}^2x$ (with t time, x horizontal coordinate, k_{er} the erosion coefficient).

The initial continental temperature field is calculated according to an age-dependent procedure (e.g., Burov and Diament, 1992), with crustal heat production $H=H_s\exp(-y/h_{\mathrm{r}})$ ($H_s=9\times10^{-10}$ W/kg, $h_{\mathrm{r}}=10$ km), and crust and mantle thermal conductivities $k_{\mathrm{c}}=k_{\mathrm{m}}=3$ W/K/m ($k=\kappa C_{\mathrm{p}}$, with specific heat $C_{\mathrm{p}}=10^3$ kJ kg^{-1} K^{-1}). The lithosphere is set to have a thermal age of 300 Ma, with temperature 1350 °C at depth 100 km. At the base of the model heat flow is prescribed to remain constant through time. The heat equation $\mathrm{d}T/\mathrm{d}t-\kappa\nabla^2T=\rho H$ is resolved (T is temperature, ρ is density), while advection is accounted for with deformation of the mesh.

Elastic–viscous–brittle rheology is modelled similarly to a number of other approaches (e.g., previous mentioned references using Parovoz), so that the brittle–ductile transition is dynamically determined. In addition to the stress field deduced from strain with the elastic constitutive law, Maxwell viscoelasticity is defined with the temperature-dependent creep law: the deviatoric shear stress $\sigma_s=[1/4(\sigma_{xx}-\sigma_{yy})^2+\sigma_{xy}^2]^{1/2}$ is obtained from the deviatoric strain rate $\mathrm{d}\varepsilon_s/\mathrm{d}t=[1/4(\mathrm{d}\varepsilon_{xx}/\mathrm{d}t-\mathrm{d}\varepsilon_{yy}/\mathrm{d}t)^2+(\mathrm{d}\varepsilon_{xy}/\mathrm{d}t)^2]^{1/2}$ through the typical relationship $\sigma_s=[(\mathrm{d}\varepsilon_s/\mathrm{d}t)/A)^{1/n}\exp(Q/nRT)]$, where A, n, Q are values extrapolated from laboratory experiences on rocks (Ranalli, 1995). Pressure-dependent brittle rheology is also assigned so that if the shear stress provided by the creep law is greater than the Mohr–Coulomb brittle yield, defined by the critical value $\tau=S_{\mathrm{o}}-\tan\phi\sigma_{\mathrm{n}}$ (where σ_{n} and τ are the normal and tangential stress, S_{o} the cohesion and ϕ the friction angle), then nonassociative failure occurs (dilatancy angle is $\psi=0$, favouring localisation; see Gerbault et al., 1998, for more detail).

The modelled lithospheric plate is divided into an upper crust, a lower crust and a lithospheric mantle, with different densities and rheological properties (Table 1). The initial crustal thickness (Moho depth) is set to Ho = 35 km, an average value for continental lithospheres (Cloetingh and Burov, 1996). There are several ways to prescribe the strength of the mantle lithosphere (Ranalli, 1995), which remains poorly constrained in nature, as illustrated by a number of recent articles (e.g., Jackson, 2002; Watts and Burov, 2003). Here, the mantle rheology is assumed to be controlled by creep

Table 1
Model density and creep power-law parameters

Layers	Density	Creep law: power n, constant A (Pa^{-n}/s), activation energy Q (J/mol)
Mantle lithosphere	3200	Olivine: n=3, $A=7\times10^4$, $Q=5.2\times10^5$
Lateral crust	2800	Quartz: n=2, $A=10^{-3}$, $Q=1.67\times10^5$ OR Mafic granulite: n=4.2, $A=1.4\times10^4$, $Q=4.45\times10^5$
Central crust	2800	Quartz: n=2, $A=10^{-3}$, $Q=1.67\times10^5$ OR Wet granite: n=1.9, $A=2\times10^{-4}$, $Q=1.37\times10^5$

Elasticity Lamé's parameters $\lambda=\mu=3\times10^{10}$ Pa. Mohr Coulomb parameters S_{o}=20 MPa, $\phi=30°$, except for the mantle lithosphere where S_{o}=200 MPa, $\psi=0°$. From compilations by various authors found in Ranalli (1995), p. 330 (Table 10.1) and p. 334 (Table 10.3).

parameters of dry olivine (Table 1), together with a maximum strength S_o=200 MPa (and zero friction), a value however that should not be considered as the physical cohesion for a rock. This cutoff value corresponds to indications provided by geophysical studies, as the average strength contrast sustainable by a relatively young (Alpine-type) lithosphere (McNutt, 1980; Lyon-Caen and Molnar, 1989; Gerbault, 2000; Gerbault et al., 2003).

3.2. Specific initial conditions

The key aspect of this modelling study is to infer the initial conditions which control variable modes of deformation in the lower crust during continental shortening. The occurrence of lateral flow and indentation must involve material that is either weak or strong enough to displace or be displaced with respect to its surroundings. For this reason we choose to incorporate a weak *central crust*. Such a weak zone mimics the heritage of a previous tectonic event: it can be of extensional/transtensional origin as suggested for the Pyrenees (Beaumont et al., 2000 and references therein) or of compressional origin as suggested for the Eastern Alps where a thermally softened preexisting orogenic wedge is inferred (Ratschbacher et al., 1991a).

The width of this prescribed weak zone is crucial: a narrow zone (~10 km wide) would simulate a preexisting localised, shearing, plate boundary, similar to the present day San Andreas fault or the Anatolian Fault. Gerbault et al. (2003) incorporated such a narrow initial weak zone when modelling the growth of the Southern Alps of New Zealand. In contrast, a weak zone several hundred kilometres wide simulates juxtaposed continental entities (or blocks) that can deform independently: for example, lithospheric-scale buckling has been proposed to occur in parts of Central Asia (e.g., Burov et al., 1993). An intermediate width of 150 km is chosen for the present modelling, which is equivalent to the reconstructed width of the preexisting late Oligocene orogenic wedge in the Eastern Alps (Frisch et al., 1998).

Taking the Eastern Alps in Europe as an example, different lines of arguments suggest that a weak zone existed prior to Late Oligocene–Miocene indentation tectonics:

(1) Metamorphic studies of the central part (hereafter called the "central wedge") of the Eastern Alps give a number of indications for weak behaviour as follows. (a) Preceding the Eocene, crustal thickening had led to amphibolite facies metamorphism (Hoinkes et al., 1999 and references therein) and to the formation of pervasive ductile fabrics (Ratschbacher et al., 1991a) in the central part of the Eastern Alps. This stacking of crustal slices may have resulted in increased radiogenic heat production and hence softening of the central wedge. (b) Subsequent exhumation of amphibolite facies rocks (e.g., Inger and Cliff, 1994; Fügenschuh et al., 1997) would have been associated with upward advection of heat, thereby cancelling the thickening related cooling signal. (c) Finally, intrusion of magmatic rocks close to the Periadric Line during the Oligocene (30–35 Ma ago) also provided heat (Sachsenhofer, 2001) from below capable of causing thermal softening.

(2) Tectonic units of Cretaceous–Oligocene age located in the central wedge may be relatively weaker than the adjacent foreland units of Variscan age, based on the concept that relative strength is linked to relative thermotectonic age (Cloetingh and Burov, 1996). This strong–weak–strong configuration is supported by rheology predictions for the geological past (Genser et al., 1996) as well as the present-day structure (Okaya et al., 1996; Willingshofer and Cloetingh, 2003). Accumulation of deformation in the central wedge is also indicative of relative weakness with respect to the foreland and the indenter (Ratschbacher et al., 1991a).

These arguments indicate that at least for the Eastern Alps, the initial central zone at the onset of Alpine compression, and representing the exhumation of metamorphic rocks together with intrusion of mafic rocks, could be simulated either by a preexisting thermal anomaly, or by a rheological heterogeneity. In the following models, we investigate the consequences of both these initial conditions. In the first case, we propose to insert a Gaussian shape of extratemperature, extending from the bottom of the model to the base of the crust. In the second case, we choose to insert a softer rheology with creep parameters A, n, Q corresponding to wet granite, while the "lateral crust" is composed of stronger material, quartz or mafic granulite (depending on models). In the second case, only the crust is softer at its centre,

to the difference of the first case, in which the central mantle lithosphere is also (thermally) softened.

3.3. Model limitations

A simple geometrical setup (Fig. 2) has been chosen, which does not necessarily reflect conditions of real orogens, but which satisfies the basic requirements for indentation and lateral flow in the lower crust. Many parameters are involved in the collision process, and here we limit ourselves to a given temperature distribution, to a constant initial crustal thickness, and to specific contrasts in rheology.

We use the Mohr–Coulomb yield criterion to model brittle failure, and power-law creep to model viscous behavior. Other constitutive laws may also be important to test, such as low temperature plasticity (Kameyama et al., 1998), strain-softening (Karato and Wu, 1993; Pysklywec et al., 2000; Gerbault et al., 2003), shear heating (Regenauer-Lieb and Yuen, 1995), or grain size-dependent creep (Gueydan et al., 2001). Furthermore, no metamorphic phase and density changes are taken into account, while in reality, they may play an important role on a time span of 20 Ma (e.g., Burov et al., 2001; Doin and Henry, 2001).

We discuss continental collision with a 2D approach, while plate tectonic deformation is fundamentally 3D. An extradimension modifies the ratio between horizontal displacements of layers and amounts of vertical thickening, which depend on equilibrium of stresses with gravity. In fact, competing factors are the amount of stress generated by the varying thickness of the crust, linked to the crust–mantle density contrast, and the strength of adjacent lithospheric layers (crust and mantle). As will be shown in the following models, horizontal deformation occurs as an alternative to vertical thickening (that competes with the gravity force). The third dimension adds the possibility to deform in 'another' horizontal direction,

Table 2
Summary of model conditions and results

	Model conditions	Surface max. height	Width over 3 km height	Lower crust	Moho depth
M1	Quartz crust+dT	3.9 km	220 km	lateral flow	54 km
M2	Crust minimum viscosity:				
	(a) 10^{20} Pa s	3.8 km	200 km	lateral flow	52 km
	(b) 10^{21} Pa s	3.6 km	130 km		50 km
	(c) 10^{22} Pa s	3.7 km	110 km		52 km
M3	Rheological weakness:				
	(a) quartz/wet granite	2 km	0 km, crustal buckling	indentation+lateral flow	42 km
	(b) mafic granulite/quartz	7 km+bulges	100 km	indentation	58 km
M4	Vertical heterogeneity:				
	(a) mafic granulite+quartz	6.5 km+bulges	100 km	indentation	60 km
	(b) 10^{23} Pa s+quartz	2.3 km	0 km		47 km
	(c) 10^{24} Pa s+quartz	6.5 km+bulges	100 km	indentation	64 km
	(d) 10^{23} Pa s+wet granite	2.8 km	0 km, central cr. buckling	indentation	50 km
M5	Other variables:				
	(a) Moho thickness=50 km	2.3 km	0 km	lateral flow	56 km
	(b) convergence=10cm/year	4 km	100 km		52 km
	(c) erosion k_{er}=1000 m^2/year	4.2 km	240 km	lateral flow	54 km

M1 is reference model with quartz crust and thermal anomaly (dT). M2 display models with similar initial conditions but with a cutoff in the minimal crustal viscosity. M3 models account for a constant geotherm but a rheological weakness. M4 models account for a constant geotherm, a rheological weakness at the center, and a vertical heterogeneity in the lateral crust. M5 models explore other parameters. Moho depth is given as measured 50 km around the centre X=0.

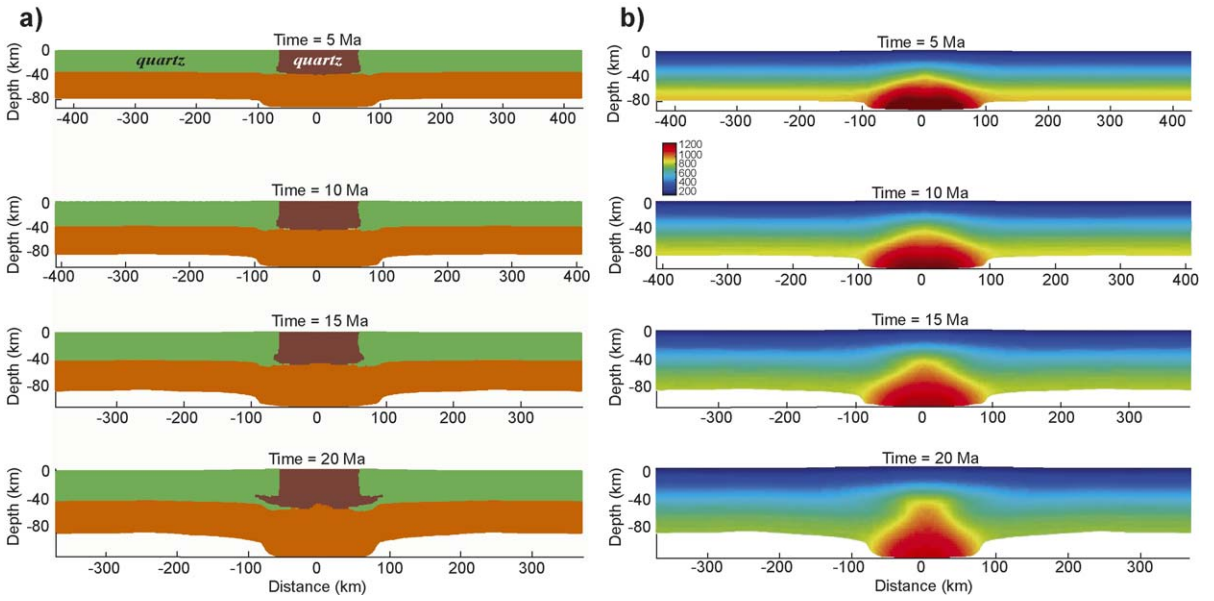

Fig. 3. Model M1 with initial central thermal anomaly after 5, 10, 15 and 20 Ma of convergence. Left panel (a) displays rheological layers with the mantle lithosphere in orange, and the crust in green and brown (with identical quartz rheologies). Right panel (b) displays the associated thermal distribution. Note the progressive change in shape from the initial Gaussian anomaly.

thus reducing the related equivalent amount of vertical thickening. Consequently, the 3D situation would only reduce the values of critical deformation and strength for which the mechanisms of indentation or horizontal flow occur, without fundamentally modifying conditions for their development.

4. Modelling results

The preexisting weakened central zone controls subsequent deformation. Sections 4.1 and 4.2 describe the evolution of models containing an initial thermal anomaly: we study conditions for lower crustal

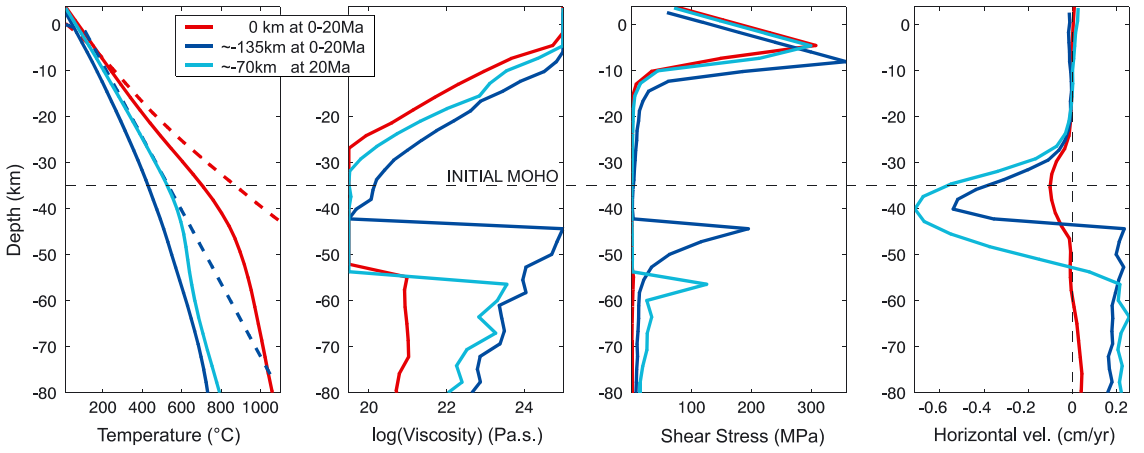

Fig. 4. Model M1 with initial central thermal anomaly after 20 Ma of convergence (dashed lines represent initial temperature profile along X=0 and X=−150 km). Temperature, viscosity, deviatoric shear stress $\{[1/4(\sigma_{xx}-\sigma_{yy})^2+\sigma_{xy}^2]^{1/2}\}$ and horizontal velocity along profiles located at the initial column X~0, −70 and −135 km. Note that areas of negative velocity occur approximately where viscosity is below 10^{21} Pa s.

horizontal flow. Sections 4.3 and 4.4 describe models with a central (or lateral) rheological heterogeneity. We study conditions for the development of indentation. Section 5 briefly recalls the known effects of varying convergence rate, erosion rate, or Moho thickness. Models conditions and results are summarised in Table 2.

4.1. A central thermal anomaly—M1

This section describes a reference model M1 in which a thermal anomaly is inserted. The thermal anomaly is defined as a Gaussian shape of additional 20 °C/km in both horizontal and vertical directions with an amplitude of 60 km centered in X=0 and Y=80 km. This results in a temperature of about 600 °C at 25 km depth and about 900 °C at 35 km depth at the Moho. In the lateral parts of the model, the 'background' temperature is equal to about 550 °C at the Moho (Fig. 3b).

Model M1 shows that from 15 to 20 Ma the central lower crust appears to displace in opposite direction to compression. Lateral flow develops in the lower crust (Fig. 3a) along an extent of nearly 50 km after 20 Ma, as indicated by negative horizontal velocities in Fig. 4, and correlates with zones of low viscosities and negligible shear stress in the lower crust.

Whereas homogeneous cooling should occur associated to homogeneous thickening (by conduction), temperatures (Fig. 3b) are affected by this gradient of horizontal deformation, and temperatures remain high at the centre. Consequently, after 15 Ma, the thermal anomaly has a plume shape, which reflects nonhomogeneous cooling rather than increasing temperatures in the centre.

Figs. 4 and 5 display vertical sections (columns) in the model: note that as the entire medium is shortened during 20 Ma, a column initially at X=−200 km ends up at position X=−165 km, and a column initially at X=−75 km ends up at X=−65 km. Shear strain associated to ductile flow does not increase much in intensity but affects a greater depth related to crustal thickening from 10 to 20 Ma (Fig. 5): at X=[−75, −65] km, outward ductile flow in the lower crust is characterised by high accumulated shear strain and high shear strain rate (Fig. 5) after 20 Ma along a thickness of 35 km. At

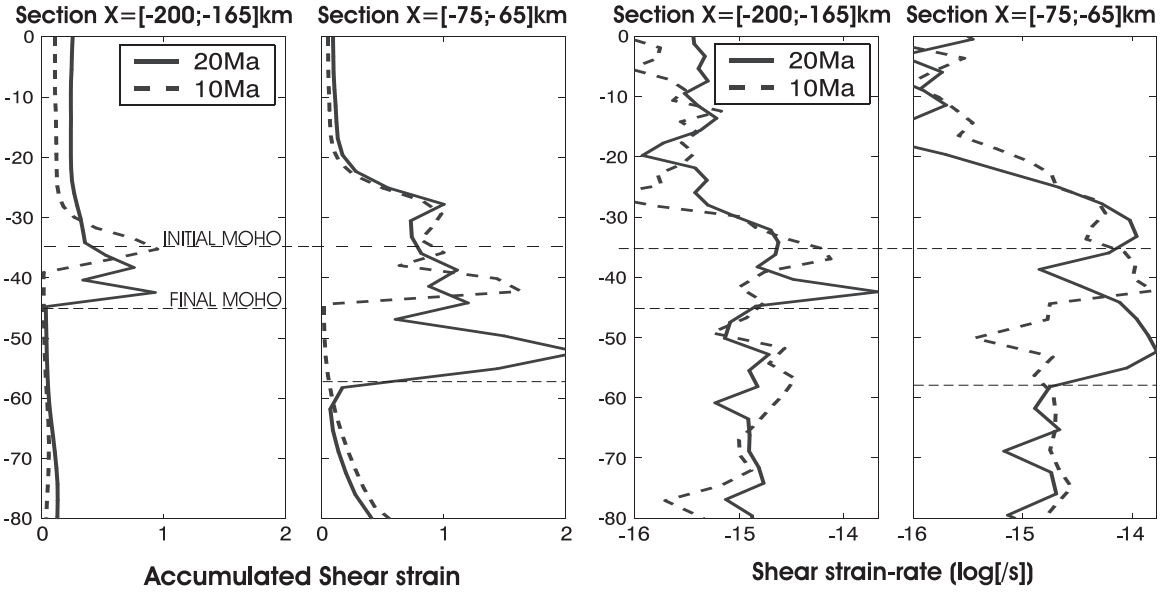

Fig. 5. Accumulated shear strain $\{[1/4(\varepsilon_{xx}-\varepsilon_{yy})^2+\varepsilon_{xy}^2]^{1/2}\}$ and shear strain rate (same but with time derivative) after 10 and 20 Ma, along three vertical profiles of M1. Note that columns "move in time' towards the centre (see titles for their initial and final positions). High strain accumulates in the ductile lower crust, along a thickness of more than 30 km at X~−75 km, and along a thickness of about 10 km at X~−200 km. Shear strain rate is highest at the edges of the lower crust rather than at its centre, illustrating a Poiseuille type of ductile flow (this is not detectable on the accumulated strain profile due to simultaneous thickening).

X=[−200, −165] km, this high shear zone affects less than 10 km thickness.

A simple approximation of horizontal displacement of the central lower crust supports our results. That is, a nearly horizontal shear strain rate of 3×10^{-15} s^{-1} integrated over a thickness of 20 km, gives a flow velocity of 0.4 cm/ year. Integrated from 10 to 20 Ma, this velocity yields a horizontal displacement of 38 km. With a minimal viscosity of 3×10^{19} Pa s, the 1D Newtonian constitutive law confirms that the associated shear stress in the lower crust is less than 1 MPa.

4.2. Condition on viscosity for ductile flow in the lower crust—M2

In model M1 (Fig. 6a), a broad topographic plateau develops by isostasy to crustal thickening (the crustal root averages to 52 km). This plateau is about 200 km wide (measured at height above 3 km), with rather moderate erosion rates around 0.1 mm/year. Such a topographic structure that develops together with channel flow in the lower crust has been extensively studied (e.g., Royden, 1996; Clark and Royden, 2000; Medvedev and Beaumont, 2001; Vanderhaeghe et al., 2003). However, here in the present models obviously the width of the plateau and of the orogen results from the initial width of the weak zone.

Up to which viscosity can the lower crust flow laterally, in opposite direction to convergence? To answer this question we modify model M1 by fixing the minimum viscosity in the lateral crust, to a cutoff value of respectively 10^{20} Pa s (M2a) , 10^{21} Pa s (M2b), 10^{22} Pa s (M2c).

Results (Figs. 6 and 7) indicate that increasing the viscosity in the lower crust prevents the development of lateral flow, and favours instead uniform thickening at the centre due to the initial thermal weakening. In other words, while low crustal viscosity (model M1) leads to a non negligible component of uniform thickening along the entire length of the model (the Moho deepens by 5 km at about 150 km away from the centre, from Fig. 4), high crustal viscosity instead (Figs. 6 and 7) leads to greater localised thickening in the centre. In model M2c, the 750 °C isotherm is advectively driven downwards due to this localised thickening, and the lateral temperature gradient diminishes.

An increase of crustal viscosity also modifies surface topography, as a mirror to crustal thickening; while low viscosity lower crust produces a typical wide and flat plateau, high viscosity produces narrower and steeper relief at the centre, and erosion rates thus increase.

4.3. A central weak rheology—M3

In this section, models M3 show the effects of a central rheological heterogeneity (150 km wide), as an alternative to a thermal anomaly (previous models M1 and M2). Within the range of values available in the literature (e.g., compilation in Ranalli, 1995), we compare three principal minerals that describe the strength of the crust, from the weakest to the strongest: wet granite, quartz, and mafic granulite. More precisely, elastic and brittle properties remain constant, and creep parameters (A, n, Q) are modified; from the weakest to the strongest dominating mineral of the crust, the viscosity is predicted to increase and the brittle–ductile transition to deepen. Therefore, we define model M3a with quartz rich lateral crust and wet granite weak central crust, and model M3b with mafic granulite lateral crust and quartz-rich central crust. The third possible case with mafic granulite and wet granite enhances deformation patterns of model M3b, since the strength contrast between both areas is greater.

M3a (Fig. 8) shows that the central crust, made of wet granite, becomes ductile at shallower depth than the lateral crust made of quartz. This leads to the development of a ‘crocodile’ geometry. At midcrustal depth, the still-brittle lateral crust “indents”, the ductile central crust. At greater depth at the base of the crust, both materials, the central and lateral crust, have again equivalent low viscosity properties, so that the central crust does not shorten as much as above. This example illustrates very well the importance of lateral strength variations, leading to depth-dependent variations in amounts of shortening.

The main mode of deformation in M3a is crustal-scale buckling, as shown by the surface topography which oscillates between 1 and 3 km height and with a wavelength equal to about 110 km (about five times the thickness of the brittle lateral crust, e.g., Gerbault et al., 1999). No significant localised relief develops in the centre, despite the presence of the weaker central

crust: this is due to uniform brittle rheology of the upper crust. Erosion rates are of the order of 0.3 mm/year. On the other hand, in the mantle lithosphere, some localised thickening is visible at the centre, as the 750 °C isotherm is progressively advected downwards. Crustal thickening is distributed over the entire width of the model, and maximum crustal thickness reaches only 42 km.

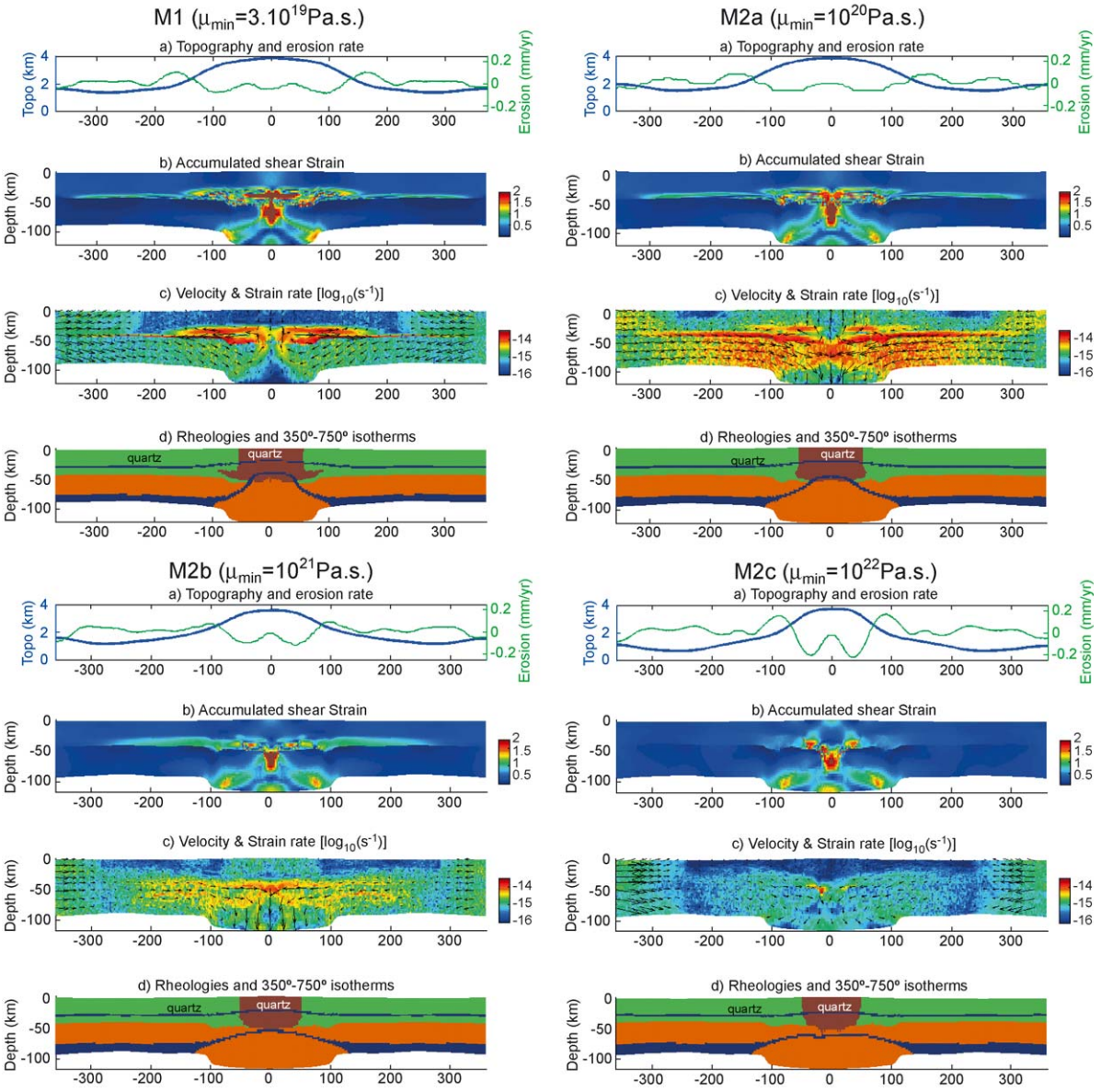

Fig. 6. Models M1 and M2 with initial central thermal anomaly after 20 Ma. Minimum cutoff viscosity is progressively increased as μ_m=3×10^{19}, 10^{20}, 10^{21}, 10^{22} Pa s. In each of the four models and from top to bottom, respectively, topography and erosion rate (which increases with increasing viscosity), the accumulated shear strain (which decreases in the lower crust far away from the centre, but increases in the central upper crust), the shear strain rate and velocity vectors (it is difficult to compare this parameter in between models since it is a snapshot at a particular time step and depends on local accelerations), and the rheological layers together with the 350 and 750 °C isotherm (which deepens at centre when cutoff viscosity increases).

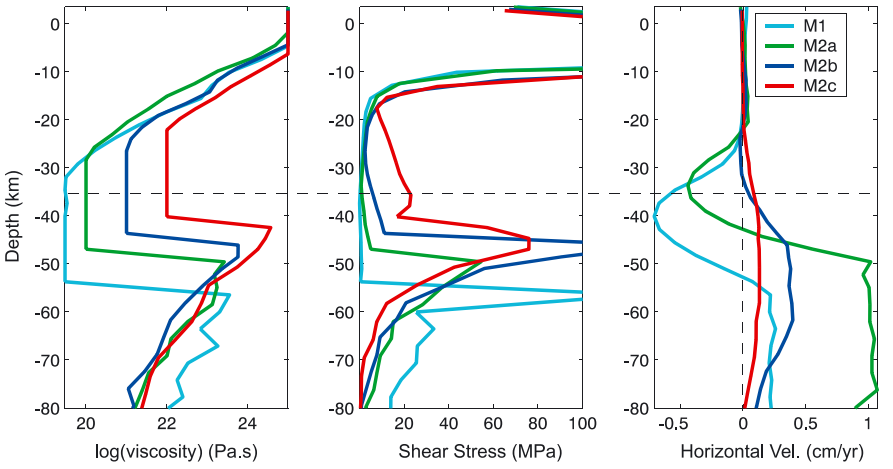

Fig. 7. Vertical profiles of viscosity, shear stress, and horizontal velocity along section X=[−75, −65] km and after 20 Ma, for models M1, M2a, M2b, M2c, in which the minimum viscosity in the lateral crust is increased. Areas of negative velocity vanish when viscosity exceeds 10^{21} Pa s and shear stress reach about 5 MPa (model M2b). Moreover, Moho depth at X=[−75, −65] km decreases with increasing minimum crustal viscosity.

Up to now, all models contained a quartz rich crust; we describe now in model M3b what happens when mafic granulite is the dominating component of the crust (A, n, Q values for the creep law). The important modification is that a mafic granulite crust with a normal geotherm (Moho temperature equal to about 550 °C) and an average strain rate around 10^{-15} s^{-1} yields minimum viscosities of the order of 10^{22} Pa s. As shown in previous models, ductile horizontal flow should not develop.

M3b (Fig. 8) shows the pattern of deformation resulting from compression of a lithosphere with a lateral crust made of mafic granulite and weaker central crust made of quartz. At depths greater than

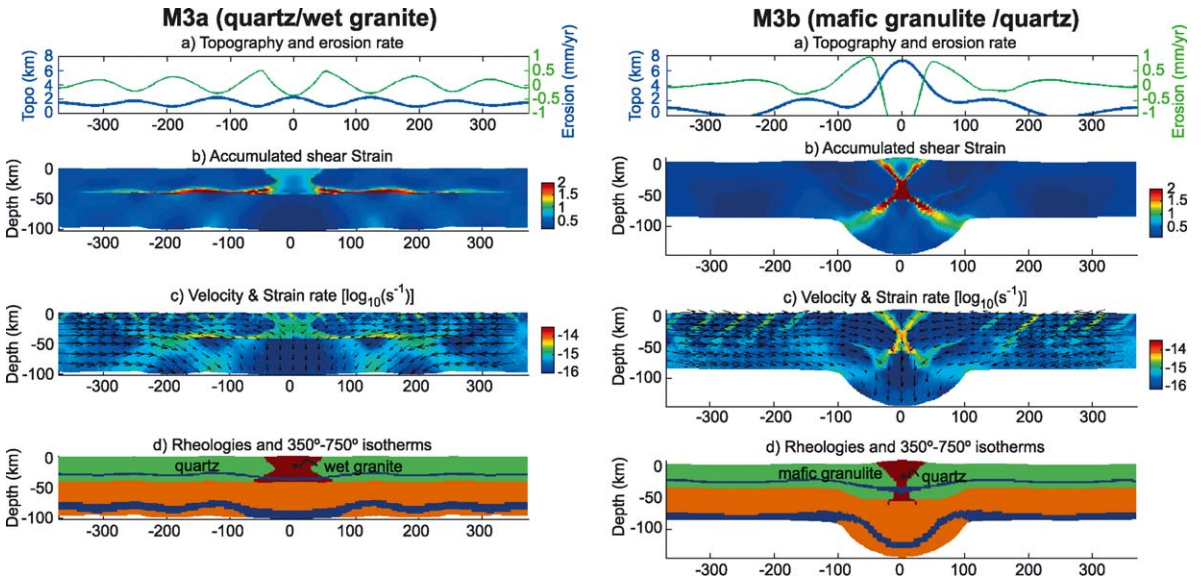

Fig. 8. M3 models with a weak central crust (and no thermal anomaly). On the left M3a, indentation of the central ductile, wet granite crust occurs in the middle crust where the lateral quartz crust is still brittle. On the right, model M3b in which the strong lateral mafic granulite crust indents the quartz central crust all the way down to the Moho, leading to a crustal scale pop-up structure.

about 15 km, the lateral resistant crust "indents" the central crust, and to the difference of model M3a, this occurs all the way down to the base of the crust. After 20 Ma, the geometry of the central crust is that of a 'cone', and shear zones localise at the boundaries of the central crust, forming a crustal-scale pop-up.

In relation to this stronger overall behaviour of the crust, both surface topography and mantle lithosphere

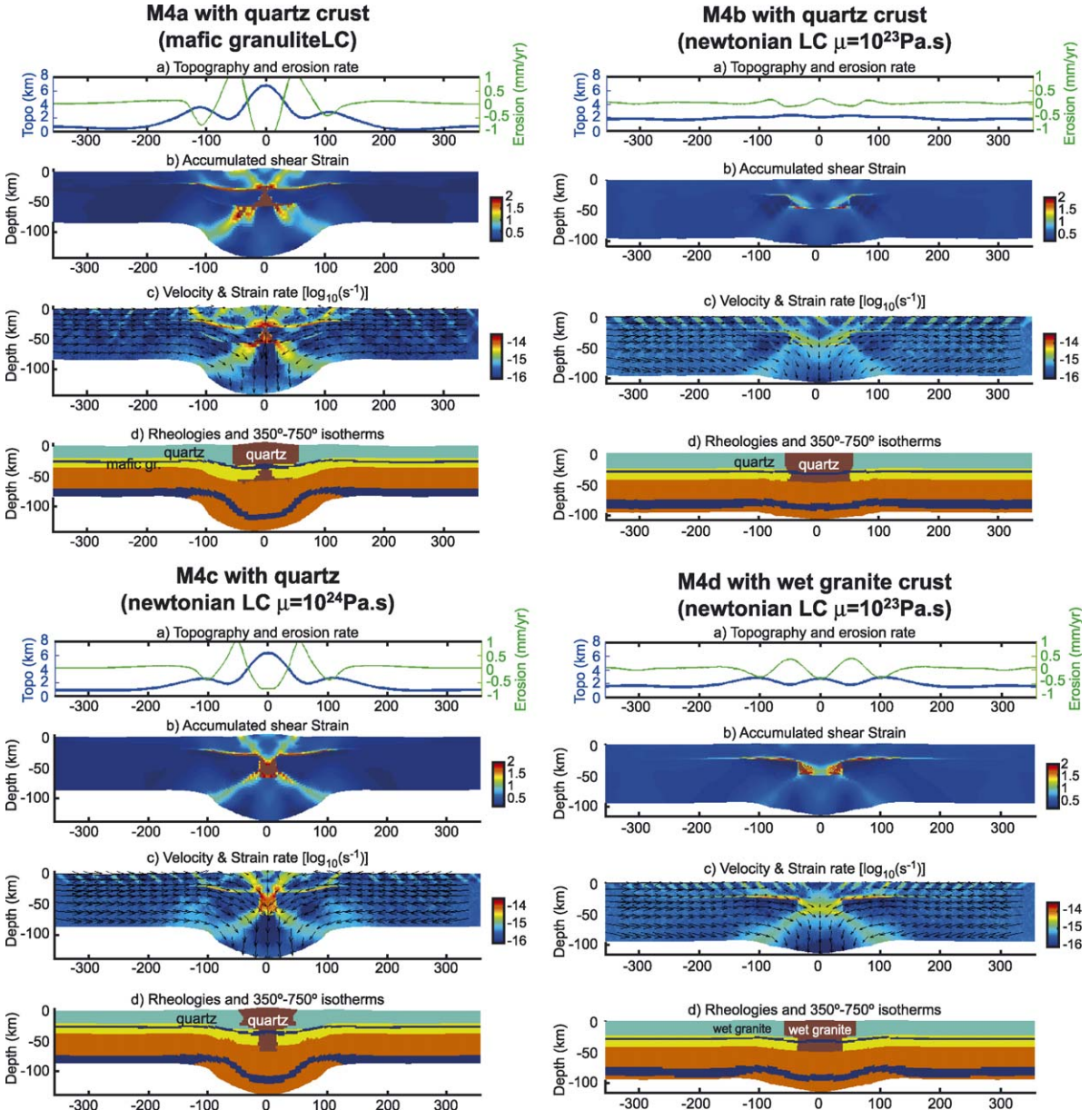

Fig. 9. Models M4, with vertical and horizontal heterogeneities. A quartz central crust and lateral upper crust (in brown and light blue), and a lower crust (LC, in yellow) of variable rheology: mafic granulite (M4a) or a Newtonian viscosity equal to 10^{23} Pa s (M4b) or 10^{24} Pa s (M4c). Model M4d is similar to M4b, with a lateral lower crust of Newtonian viscosity equal to 10^{23} Pa s, but the central crust is now composed of wet granite central crust (in brown): in comparison to M4a the latter concentrates more shortening.

display important vertical deformation. Relief is high (7 km), with steep slopes and thus high erosion rates (1 mm/year). The crustal root develops to about 60 km depth over a distance equivalent to the initial width of the rheological anomaly.

Topography also displays secondary forebulges related to flexural bending of the lithosphere. This flexure is now significant because it is related to the thickness of coupled mantle and crust behaving as a single strong layer (Burov and Diament, 1992). Erosion rates are about one order of magnitude higher than in previous models with a quartz crust. These results are comparable to previous models that studied local folding of the continental lithosphere as a precursor for orogeny (e.g., Burg and Podladchikov, 1999).

4.4. Condition for indentation of the central crust—M4

Previous model M3b, with mafic granulite lateral crust, showed that weak material at the centre gets squeezed, as it is indented by portions of lateral lower crust of higher viscosity. In this section, we seek for a model capable of developing more typical indentation features in the crust.

In model M4a, we introduce a vertical heterogeneity in the crust: the upper crust (light blue in Fig. 9) has quartz creep parameters, and the lower crust has mafic granulite creep parameters (in yellow). In the centre, quartz rheology is taken, so that there is also a lateral heterogeneity in the lower crust between quartz central crust surrounded by mafic granulite lateral crust.

In this case, the strong lateral lower crust (yellow in Fig. 9) behaves as a horizontal indenter. That is, it detaches from the upper crust (ductile base of the upper crust) to move rigidly towards the centre.

Similarly to M3b and since the lateral crust is strong at depth, deformation accumulates in shear zones that border the central crust, isolating this central portion to form a crustal-scale pop-up structure. The lithosphere also bends as single strong layer, producing steep and narrow topography bordered by flexural bulges.

We then test which minimum viscosity can make the lateral lower crust act as a 'rigid' indenter. Model M4b (Fig. 9) is a 'critical' stage, in which the lateral lower crust, in yellow in figures, behaves as a layer of constant newtonian viscosity equal to 10^{23} Pa s. This model shows a little indentation (over a distance less than 10 km). Below this viscosity, there is uniform deformation and crustal buckling similar to model M3a, whereas above at 10^{24} Pa s (M4c), the situation resembles M4a.

Model M4d is similar to M4b (Fig. 9), with a lateral lower crust composed of material at viscosity 10^{23} Pa s, but the upper crust and the central crust (in light blue and brown) are now composed of wet granite, instead of quartz. In this case, viscosity contrasts are higher than in M4b, and indentation occurs.

5. Discussing other parameters

This section briefly recalls how other parameters are expected to control the occurrence of either lateral flow or indentation structures during continental orogeny. Previous modelling studies have already demonstrated in detail the influence of the geotherm (or thermal age), the convergence rate and the Moho thickness on the strength of the lithosphere (e.g., Cloetingh and Burov, 1996). The role of surface processes on orogenic evolution has also been studied (e.g., Beaumont et al., 1992, 1996; Avouac and Burov, 1996; Willett, 1999). Therefore, it is not our aim here to redemonstrate these effects. Yet, the discussion below emphasizes that the modification of a single parameter leads to multiple thermal and mechanical effects on the dynamical balance of forces, and hence on the ratio of horizontal and vertical patterns of deformation. Therefore, the additional models that we display constitute only a sample amongst a wide range of possible solutions, which strongly depend on the combination of all parameters.

5.1. Crustal thickness

Increasing the crustal thickness (greater than 35 km) can predict to have two opposite consequences:

– A depth increase of crustal rocks increases their temperature, and therefore decreases their viscosity. Thus, lateral flow should occur over a greater crustal thickness and develop over a greater horizontal extent. Such a case could be compared to areas such as the Altiplano–Puna or Tibet, in which a thick

crust is present within a relatively warm temperature field (model M5a, Fig. 11).

– However, thick continental crust is generally associated with old (e.g., Paleozoic) regions with low geothermal gradients and a rather dominant mafic composition (e.g., Cloetingh and Burov, 1996). In such cases, very little if at all, lateral flow should occur, because the viscosity at lower crustal depths should be greater than 10^{22} Pa s.

5.2. Convergence rate

Increasing the rate of convergence decreases viscosity contrasts, and has the following consequences:

– A first effect is that the average strain rate in the entire lithosphere is increased: according to the power law creep constitutive law, this increases the viscosity. Consequently, lateral flow is inhibited (resembling models M3).

– The temperature distribution is also modified. Where there is a local (central) thermal anomaly like in models M1 and M2, horizontal advection of cold temperatures towards the warmer centre is enhanced. The central weak zone thus vanishes together with the central thermal anomaly, inhibiting localised deformation and ductile flow (model M5b, Fig. 11).

5.3. Erosion rate

Removal or addition of material at the surface modifies the weight of a column of crust. Since an increase in surface processes increases removal of material at the centre where relief is highest, we expect the following implications:

– Increased erosion at the centre facilitates exhumation. Therefore, uniform vertical deformation (thickening) is eased to the expense of horizontal flow. On the other hand, fast exhumation also uplifts isotherms and reduces viscosities at the centre, which facilitates lateral flow (e.g., Beaumont et al., 2001, Vanderhaeghe et al., 2003).

– At the flanks of the orogen, erosion and sedimentation tend to homogenise surface relief. Below in the lower crust, crustal thickening by horizontal flow is sensitive to this change in distribution of masses. As lateral flow thickens the crust, isostasy implies the rise of compensated relief: surface processes may thus act against the building of this compensated relief, and prevent the development of lateral horizontal flow (e.g., Avouac and Burov, 1996).

Model M5c (Fig. 11) displays a model similar to M1 with a coefficient of erosion multiplied by 10. The geometry of deformation does not significantly change in this situation, as the effects presented above seem to equilibrate.

6. Implications for the evolution of collision zones and conclusions

We developed models of continental collision by shortening a continental lithosphere with a central weak zone 150 km wide. The results after 20 Ma show that initial lateral strength variations in the crust, due to either thermal anomalies or crustal compositional changes, have far reaching consequences for the distribution of strain and overall geometry of the orogeny, linking in particular (a) the strength and viscosity in the lower crust, and (b) the shape of surface topography and Moho.

In addition to a scenario of uniform shortening and thickening of the crust under applied compression, two fundamentally different scenarii of deformation can occur: horizontal ductile flow of the

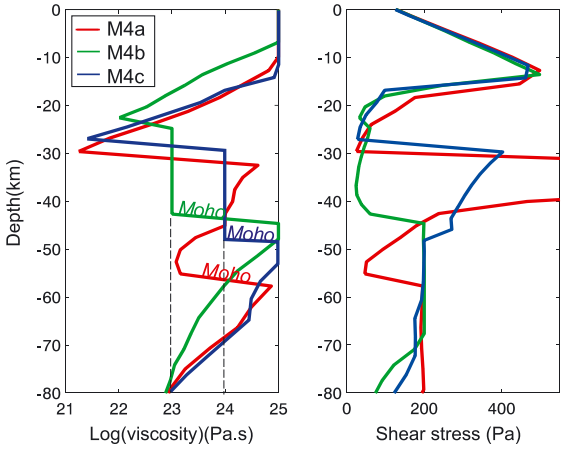

Fig. 10. Vertical profiles of viscosity and deviatoric shear stress along column X~−65 km in the lateral crust, for models M3b, M4a, M4b and M4c. For a quartz-rich crust, the brittle–ductile transition occurs between 10 and 15 km depth. Viscosity and strength at this depth, down to the Moho, control the overall pattern of deformation (indentation features). When the strength of the lower crust is greater than approximately 50 MPa, indentation may occur.

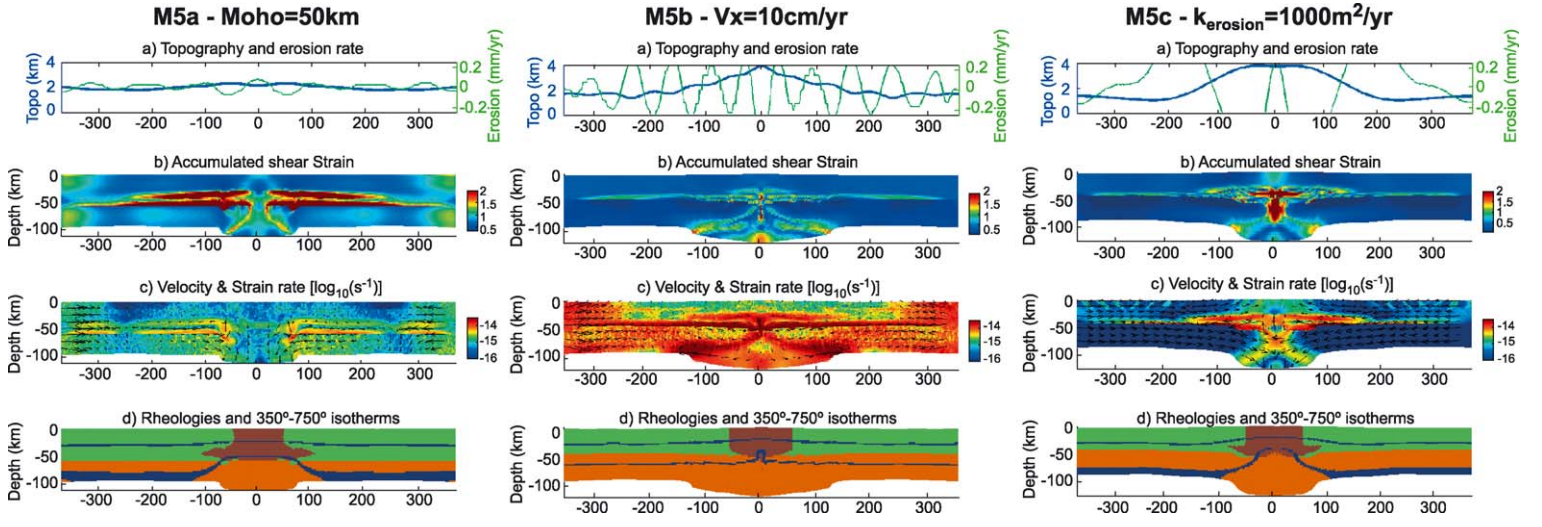

Fig. 11. M5 models similar to M1, with uniform quartz crust and a thermal anomaly. From left to right, model M5a, with an initial crustal thickness of 50 km: lateral flow occurs over a distance of 300 km. In M5b, increased convergence rate (10 cm/year) reduces viscosity contrasts, reduces the central thermal anomaly and favours uniform deformation. In M5c, the erosion coefficient has been multiplied by 10. There are no significant changes due to balancing effects of increased exhumation rate at the centre and erosion of relief that builds by isostasy.

central lower crust, when viscosities are lower than 10^{21} Pa s (models M1 M2a; Figs. 3, 6 and 7), or indentation of the central crust by lateral lower crust, when viscosities are greater than 10^{23} Pa s (models M4, Figs. 10 and 11):

– Crustal thickening associated to lower crust ductile flow against the direction of shortening is obtained for quartz rich lower crust (or weaker power-law creep conditions). Channel flow is evidenced by subhorizontal shear zones that develop in the lower crust below the brittle–ductile transition zone and right above the base of the Moho (similar to Bird, 1991; Shen et al., 2001; Medvedev and Beaumont, 2001; Vanderhaeghe et al., 2003). Whereas the applied compression strain rate is 10^{-16} s^{-1}, strain rates in the lower crust exceed 3×10^{-15} s^{-1} in the flow channel, producing differential displacements of several tens of kilometres. This mode of deformation results in *outward pointing wedges*.

– Indentation of the central weak crust by strong lateral crust is best obtained when we account for a vertical rheological layering of the upper and lower crust, with contrasts in viscosities of at least 2 orders of magnitude. Then the strong lateral lower crust, composed of mafic granulite or with a Newtonian viscosity of at least 10^{23} Pa s (it may thus remain ductile), indents and squeezes the central weaker crust to produce *inward pointing wedges*.

These two opposite behaviours of the lower crust produce typically different patterns of deformation, surface relief and crustal root:

– In cases of shortening being accommodated by horizontal ductile flow in the lower crust, deformation is taken up within a wider zone than the initial 150 km, and the resulting topography is characterised by gentle slopes and a fairly flat plateau-like shape above height 3 km. Thus, erosion rates are low to moderate (lower than 0.2 mm/year). Conversely, Moho topography is smooth and describes a crustal root zone about 200 km wide and 50 km deep.

– In contrast, a strong lateral lower crust favours strain localisation into narrow crustal-scale shear zones at the boundary of the weak and strong crusts, and define a huge pop-up which uplifts the central crust. Accordingly, surface topography is characterised by steep slopes at the centre, flanked by flexural bulges. These steep slopes are responsible for relatively high erosion rates (greater than 0.5 mm/year). At depth, the crustal root can exceed 60 km locally, in a narrow zone less than 60 km wide. Such a narrow zone of deep crustal material maintains there because it is squeezed by the mantle and crust both acting as a single, strong layer (see also Cloetingh and Burov, 1996; Burg and Podladchikov, 1999).

Our choices of rheology and boundary conditions result in critical viscosities of the lower crust, 10^{21} Pa s for ductile flow and 10^{23} Pa s for indentation, that can be compared with other studies, and despite variable modelling assumptions. A number of models have been developed to explore conditions for the development of high topographic plateaus such as the Altiplano–Puna or Tibet. Although our study had different goals (we trigger plateau development by inserting a weak zone already 150 km wide), the critical value that we obtain is comparable with these analytical or numerical studies (e.g., Royden et al., 1997; Shen et al., 2001; Medvedev and Beaumont, 2001; Husson and Ricard, 2004; Vanderhaeghe et al., 2003).

Crocodile structures referring to wedge shapes of imbricate layers are often observed, not only on the field (e.g., in the Svecofennian orogen, Beunk and Page, 2001) but also on seismic images, as oppositely dipping reflectors, such as in the Eastern Alps, for example (Model A in TRANSALP Working Group, 2002). Our study shows that such geometries can result from either horizontal ductile flow at low stress (less than about 5 MPa, Fig. 7) producing ‘outward pointing wedges’, or from indenting lower crust at high stress (greater than about 50 MPa, Fig. 10), associated to ‘inward pointing wedges’.

Naturally, the lithospheric structure (layers geometries, geotherm, and rock composition) and the boundary conditions (convergence rate and surface processes) of a specific area should first be constrained at best with data, in order to reasonably assess the occurrence of lower crustal lateral flow or indentation within a collision zone. Although the viscosity and strength of the lower crust are not directly measurable quantities, careful analyses of different data sets (topography, gravity, heat flow, strain markers, gravity, seismics) help to constrain crustal rheology. In this view, the following step to this study is an application to the Eastern Alps.

Acknowledgements

This work initiated at Vrije Universiteit in Amsterdam in 2001, with a postdoctoral funding by the ISES programme for M.G., and continued at the LMTG of Toulouse: these institutions are thanked for providing technical support. E.W. acknowledges funding of this study by NWO, the Netherlands Organization for Scientific Research, project 810.31.003. We thank reviewers for their constructive remarks that improved the focus of the paper.

Appendix A. ANNEX: characterising the geometry of modelled orogens

Vanderhaeghe et al. (2003) developed models of orogenic growth over a subducting mantle lithosphere and proposed to characterise "double-wedge" and "plateau" types of evolution in terms of two parameters: K_p the plateau coefficient, and E_t the effective width of thickening (Fig. 1A).K_p, the plateau coefficient, characterises the shape of the surface topography in comparison to a perfect plateau (see Vanderhaeghe et al., 2003, for calculation). K_p=1 for a perfect plateau and K_p=0.5 for a perfect double-wedge. Vanderhaeghe et al. (2003) argue that K_p=0.65 is indicative of onset of plateau-like behaviour. In comparison, our models give K_p=0.6 as indicative of the onset of lateral lower crustal flow (our models M1, M2a, viscosity lower than 10^{21} Pa s, Fig. 6).

E_t, the effective width of thickening, measures the distribution of crustal thickening, and is defined as the virtual width of a zone of constant crustal thickness equal to the real maximum crustal thickness H_m. E_t tends to reach a constant value in the plateau stage (Vanderhaeghe et al., 2003). For this study we estimate E_t at each time in comparison to the initial stage. Our models show that E_t increases slowly to values greater than 150 km (the initial width of our modelled orogens) when lateral lower crustal flow occurs.

Assumptions differ in many ways between Vanderhaeghe et al. (2003) and our modelling approach. Most importantly, the former study assumes discontinuous and asymmetric velocity boundary condition at the base of the crust, mimicking subduction of mantle lithosphere. In addition, rheological parameters differ, with a greater density contrast between the crust and the mantle, a lower crustal friction angle, and no elastic component of deformation. All these values are involved in the balance of forces during convergence, that is, according to the formalism of Vanderhaeghe et al. (2003), the equilibrium of gravity force F_g, compressional force F_c, and resistance of the crust against the mantle or basal traction F_t:F_g+F_c=F_t. In our case, F_g and F_c apply to the entire scale of the modelled lithosphere, and F_t should be considered as an internal resistance of the crust at its evolving boundary with the mantle. For all these reasons, it is not surprising that our interpretation of critical values for K_p and E_t differ.

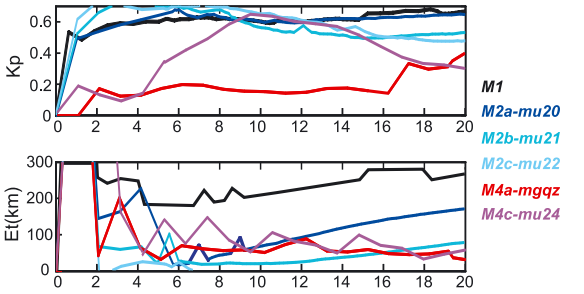

Fig. 1A. Plateau coefficient (K_p) and Effective width of thickening (E_t) for models M1, M2 and M4: K_p greater than 0.6, and E_t increasing slowly to a value greater than 150 km are features coherent with lateral lower crustal flow.

References

Artyushkov, E.V., 1973. Stresses in the lithosphere caused by crustal thickness inhomogeneities. J. Geophys. Res. 78, 7675–7708.

Avouac, P., Burov, E.B., 1996. Erosion as a driving mechanism of intracontinental mountain growth. J. Geophys. Res. 101, 17747–17769.

Beaumont, C., Fullsack, P., Hamilton, J., 1992. Erosional control of active compressional orogens. In: Clay, M.C. (Ed.), Thrust Tectonics. Chapman and Hall, New York, pp. 1–31.

Beaumont, C., Kamp, P.J., Hamilton, J., Fullsack, P., 1996. The continental collision zone South Island, New Zealand: comparison of geodynamical models and observations. J. Geophys. Res. 101, 3333–3359.

Beaumont, C., Munoz, J.A., Hamilton, J., Fullsack, P., 2000. Factors controlling the Alpine evolution of the central Pyrenees inferred from a comparison of observations and geodynamical models. J. Geophys. Res. 105, 8121–8145.

Beaumont, C., Jamieson, R.A., Nguyen, M.H., Lee, B., 2001. Himalayan tectonics explained by extrusion of a low-viscosity crustal channel coupled to focused surface denudation. Nature 414, 738–742.

Beunk, F.F., Page, L.M., 2001. Structural evolution of the accretional continental margin of the paleoproterozoic Svecofennian orogen in Southern Sweden. Tectonophysics 339, 67–92.

Bird, P., 1991. Lateral extrusion of lower crust from under high topography, in the isostatic limit. J. Geophys. Res. 96 (6), 10275–10286.

Brace, W.F., Kohlstedt, D.L., 1980. Limits on lithospheric stress imposed by laboratory experiments. J. Geophys. Res. 85, 6248–6252.

Buck, W.R., Poliakov, A., 1998. Abyssal hills formed by stretching oceanic lithosphere. Nature 392, 272–275.

Burg, J.-P., Podladchikov, Y., 1999. Lithospheric scale folding: numerical modelling and application to the Himalayan syntaxes. Int. J. Earth Sci. 88, 190–200.

Burov, E.B., Diament, M., 1992. Flexure of the continental lithosphere with multilayered rheology. Geophys. J. Int. 109, 449–468.

Burov, E., Poliakov, A., 2001. Erosion and rheology controls on synrift and postrift evolution: verifying old and new ideas using a fully coupled numerical model. J. Geophys. Res. 106, 16461–16481.

Burov, E.B., Lobkovsky, L.I., Cloetingh, S., Nikishin, A.M., 1993. Continental lithosphere folding in Central Asia: constraints from gravity and topography. Tectonophysics 226, 73–87.

Burov, E., Jolivet, L., Le Pourhiet, L., Poliakov, A., 2001. A thermomechanical model of exhumation of high pressure (HP) and ultra-high pressure (UHP) metamorphic rocks in Alpine-type collision belts. Tectonophysics 342, 113–136, 6450.

Chery, J., Vilotte, J.-P., Daignieres, M., 1991. Thermomechanical evolution of a thinned continental lithosphere under compression; implications for the Pyrenees. J. Geophys. Res. 96, 4385–4412.

Clark, M.K., Royden, L.H., 2000. Topographic ooze: building the eastern margin of Tibet by lower crustal flow. Geology 28, 703–706.

Cloetingh, S., Burov, E.B., 1996. Thermomechanical structure of the European continental lithosphere: constraints from rheological profiles and EET estimates. Geophys. J. Int. 124, 695–723.

Cundall, P., Board, M., 1988. A microcomputer program for modelling large-strain plasticity problems. Numer. Methods Geomech. 6, 2101–2108.

Davy, P., Cobbold, P.R., 1988. Indentation tectonics in nature and experiment: 1. Experiments scaled for gravity. Bull. Geol. Inst. Univ. Upps., NS 14, 129–141.

Deichmann, N., 1992. Structural and rheological implications of lower-crustal earthquakes below northern Switzerland. Phys. Earth Planet. Inter. 69, 270–280.

Doin, M.P., Henry, P., 2001. Subduction initiation and continental crust recycling; the roles of rheology and eclogitization: exhumation of high-pressure rocks; kinetic, thermal and mechanical constraints. Tectonophysics 342, 163–191.

Frisch, W., Kuhlemann, J., Dunkl, I., Brügel, A., 1998. Palinspastic reconstruction and topographic evolution of the Eastern Alps during late Tertiary tectonic extrusion. Tectonophysics 297, 1–15.

Fügenschuh, B., Seward, D., Mancktelow, N., 1997. Exhumation in a convergent orogen: the western Tauern window. Terra Nova 9, 213–217.

Genser, J., van Wees, J.D., Cloetingh, S., Neubauer, F., 1996. Eastern Alpine tectono-metamorphic evolution; constraints from two-dimensional *P–T–t* modeling. Tectonics 15, 584–604.

Gerbault, M., 2000. At what stress level is the Indian Ocean lithosphere buckling? Earth Planet. Sci. Lett. 178, 165–181.

Gerbault, M., Poliakov, A.N.B., Daignières, M., 1998. Predition of faulting from the theories of elasticity and plasticity; what are the limits? J. Struct. Geol. 20, 301–320.

Gerbault, M., Burov, E.B., Poliakov, A.N.B., Daignières, M., 1999. Do faults trigger folding in the lithosphere? Geophys. Res. Lett. 26, 271–274.

Gerbault, M., Henrys, S., Davey, F., 2003. Numrical models of lithospheric deformation forming the Southern Alps of New Zealand. J. Geophys. Res. 108, 2341.

Goetze, C., 1978. The mechanism of creep in olivine. Philos. Trans. R. Soc. Lond. Ser. A: Math. Phys. Sci. 288, 99–119.

Gratton, J., 1989. Crustal shortening, root spreading, isostasy, and the growth of orogenic belts: a dimensional analysis. J. Geophys. Res. 94, 15627–15634.

Gueydan, F., Leroy, Y.M., Jolivet, L., 2001. Grain-size-sensitive flow and shear-stress enhancement at the brittle–ductile transition of the continental crust. Int. J. Earth Sci. 90-1, 181–196.

Hill, R., 1950. The Mathematical Theory of Plasticity. Oxford Engineering Science Series 11. Oxford University Press, Oxford, UK.

Hoinkes, G., Koller, F., Rantitsch, G., Dachs, E., Hack, V., Neubauer, F., Schuster, R., 1999. Alpine metamorphism of the Eastern Alps. Schweiz. Mineral. Petrogr. Mitt. 79, 155–181.

Husson, L., Ricard, Y., 2004. Stress balance above subduction zones - application to the Andes. Earth Planet. Sci. Lett. 222 (3–4), 1037–1050.

Inger, S., Cliff, R.A., 1994. Timing of metamorphism in the Tauern Window, Eastern Alps: Rb–Sr ages and fabric formation. J. Metamorph. Geol. 12, 695–707.

Jackson, J., 2002. Strength of the continental lithosphere: time to abandon the jelly sandwich? GSA Today 12 (9), 4–9.

Kameyama, M.C., Yuen, D., Karato, S.-I., 1998. Thermal-mechanical effects of low-temperature plasticity (Pierls mechanism) on the deformation of a visco-elastic shear zone. Earth Planet. Sci. Lett. 168, 159–172.

Karato, S., Wu, P., 1993. Rheology of the upper mantle: a synthesis. Science 260, 771–778.

Klemperer, S.L., 1987. A relation between continental heat flow and the seismic reflectivity of the lower crust. J. Geophys. 61, 1–11.

Lobkovsky, L.I., Kerchmann, V.I., 1991. A two level concept of plate tectonics: application to geodynamics. Tectonophysics 199, 343–374.

Lyon-Caen, H., Molnar, P., 1989. Constraints on the deep structure and dynamic processes beneath the Alps and adjacent regions from an analysis of gravity anomalies. Geophys. J. R. Astron. Soc. 99, 19–32.

McKenzie, D., Nimmo, F., Jackson, J.A., Gans, P.B., Miller, E.L., 2000. Characteristics and consequences of flow in the lower crust. J. Geophys. Res. 105, 11029–11046.

McNutt, Marcia, 1980. Implications of regional gravity for state of stress in the earth's crust and upper mantle. J. Geophys. Res. 85, 6377–6396.

Medvedev, S., Beaumont, C., 2001. Growth of continental plateaux: channel injection or tectonic thickening? AGU Fall Meeting, San Francisco, USA. EOS Transactions.

Odé, H., 1960. Faulting as a velocity discontinuity in plastic deformation. Mem. Geol. Soc. Am. 79, 293–321.

Okaya, N., Cloetingh, S., et al., 1996. A lithospheric cross section through the Swiss Alps (part II): constraints on the mechanical structure of a continent–continent collision zone. Geophys. J. Int. 127, 399–414.

Ord, A., Hobbs, B.E., 1989. The strength of the continental crust, detachment zones and the development of plastic instabilities. Deformation of Crustal Rocks, Tectonophysics, vol. 158. pp. 269–289.

Pfiffner, O.A., Ellis, S., et al., 2000. Collision tectonics in the Swiss Alps: insight from geodynamic modeling. Tectonics 19, 1065–1094.

Poliakov, A., Podladchikov, Y., 1992. Diapirism and topography. Geophys. J. Int. 109, 553–564.

Pysklywec, R., Beaumont, C., Fullsack, P., 2000. Modeling the behavior of the continental mantle lithosphere during plate convergence. Geology 28, 655–658.

Ranalli, G., 1995. Rheology of the Earth, 2nd ed. Chapman and Hall, London. 413 pp.

Ratschbacher, L., Merle, O., et al., 1991. Lateral extrusion in the eastern Alps: Part 1. Boundary conditions and experiments scaled for gravity. Tectonics 10, 245–256.

Ratschbacher, L., Frisch, W., et al., 1991. Lateral extrusion in the eastern Alps: Part 2. Structural analysis. Tectonics 10, 257–271.

Regenauer-Lieb, K., 1999. Dilatant plasticity applied to Alpine Collision: ductile void growth in the intraplate area beneath the Eifel Volcanic Field. J. Geodyn. 27, 1–21.

Regenauer-Lieb, K., Yuen, D., 1995. Rapid conversion of elastic energy into shear heating during incipient necking of the lithosphere. J. Geophys. Res. Lett. 25, 17587–17602.

Ross, A.R., Brown, L., Pananont, P., Nelson, K.D., Klemperer, S., Haines, S., Wenjin, Z., Jingru, G., 2004. Deep reflection surveying in central Tibet: lower-crustal layering and crustal flow. Geophys. J. Int. 156, 115–228.

Royden, L.H., 1996. Coupling and decoupling of crust and mantle in convergent orogens: implications for strain partitioning in the crust. J. Geophys. Res. 101, 17679–17705.

Royden, L.H., Burchfiel, C., King, R.W., Wang, E., Chen, Z., Shen, F., Liu, Y., 1997. Surface deformation and lower crustal flow in Eastern Tibet. Science 276, 788–790.

Sachsenhofer, R.R., 2001. Syn- and post-collisional heat flow in the Cenozoic Eastern Alps. Int. J. Earth Sci. 90, 579–592.

Schmid, S.M., Kissling, E., 2000. The arc of the western Alps in the light of geophysical data on deep crustal structure. Tectonics 19, 62–85.

Shen, F., Royden, L.-H., Burchfiel, B.-C., 2001. Large-scale crustal deformation of the Tibetan Plateau. J. Geophys. Res. 106-4, 6793–6816.

Tapponnier, R., Peltzer, G., Le Dain, A.Y., Armijo, R., Cobbold, P., 1982. Propagating extrusion tectonics in Asia; new insights from simple experiments with plasticine. Geology 10 (12), 611–616.

Thompson, A.B., Schulmann, K., Jezek, J., 1997. Extrusion tectonics and elevation of lower crustal metamorphic rocks in convergent orogens. Geology 25, 491–494.

TRANSALP Working Group, 2002. First deep seismic reflection images of the Eastern Alps reveal giant crustal wedges and transcrustal ramps. Geophys. Res. Lett. 29 (10) doi:10.10129/2002GL014911.

Vanderhaeghe, O., Medvedev, S., Beaumont, C., Jamieson, R.A., 2003. Evolution of orogenic wedges and continental plateaux: insights from crustal thermal-mechanical models overlying subducting mantle lithosphere. Geophys. J. Int. 153, 27–51.

Watts, A.B., Burov, E.B., 2003. Lithospheric strength and its relationship to the elastic and seismogenic layer thickness. Earth Planet. Sci. Lett. 213, 113–131.

Willett, S.D., 1999. Orography and orogeny: the effects of erosion on the structure of mountain belts. J. Geophys. Res. 104, 28957–28981.

Willingshofer, E., Cloetingh, S., 2003. Present-day lithospheric strength of the eastern Alps and its relationship to neotectonics. Tectonics 22, 1075.